

Practical joint domain localised adaptive processing in homogeneous and nonhomogeneous environments.

Part 2: Nonhomogeneous environments

R.S.Adve, T.B.Hale and M.C.Wicks

Abstract: The second part of this two-part paper deals with space-time adaptive processing (STAP) in nonhomogeneous environments. This paper introduces a new two-dimensional non-statistical, direct data domain (D^3) STAP algorithm and a hybridisation of this D^3 approach with the joint domain localised (JDL) algorithm. The D^3 algorithm replaces the non-adaptive transform used in Part 1 thereby suppressing discrete interference. A second stage of statistical processing in the angle-Doppler domain suppresses residual correlated interference. This new two-stage hybrid STAP technique allows for the application of the JDL algorithm within range cells determined to be nonhomogeneous. The development here draws heavily on the formulation presented in Part 1 of this paper. The work presented brings together two different aspects of STAP research: statistical and D^3 processing. In doing so, this research fulfils an important need in the context of practical STAP, particularly knowledge-based algorithms. The envisioned system uses multi-pass processing to determine key information regarding the interference scenario. Depending on the homogeneity of the interference, the algorithm in Part 1 or that in Part 2 of the paper may be used.

1 Introduction

Classical space-time adaptive processing (STAP) algorithms achieve interference suppression using the interference covariance matrix, typically estimated using secondary data from range cells close to the primary range cell under test. The assumption is that the secondary data samples are independent and identically distributed (i.i.d.) with respect to the interference in the range cell under test, i.e. the data is homogeneous. The performance of statistical algorithms suffers significantly when the data is nonhomogeneous, that is when the secondary data does not reflect the statistics of the interference in the primary range cell.

In practice, the assumption of homogeneous data is routinely violated. For example, urban areas and land-sea interfaces present the problem of large variations in terrain over relatively short distances. The corresponding fluctuation in clutter statistics undermines the accuracy of the covariance matrix estimate and, in turn, the detection performance. Statistical algorithms may be applied in these cases, however the probability of detection falls and the probability of false alarm increases. These algorithms reach their performance potential only within those regions where the interference is homogeneous.

It is impossible to know *a priori* which range cells within the data cube are homogeneous and which are not. Therefore practical adaptive processing requires a multi-pass scheme. The first pass uses a nonhomogeneity detector (NHD) to separate target detection into two categories: detection within homogeneous range cells and within nonhomogeneous range cells.

Performance degradation of STAP algorithms due to nonhomogeneous data occurs in two forms. In one form the secondary data is not i.i.d., leading to an inaccurate estimate of the covariance matrix. For example, the clutter statistics in urban environments fluctuate rapidly with distance, i.e. range cells. To minimise the loss in performance due to nonhomogeneous sample support, a NHD may be used to identify secondary data cells that do not reflect the statistical properties of the primary data. These data samples are then eliminated from the estimate of the covariance matrix. A discussion of NHDs is provided elsewhere [1-4] and is not repeated here. In particular, Chang [1] presents both the generalised inner product (GIP) and modified sample matrix inverse (MSMI) NHDs and is a good introduction to this research topic.

The second form of performance loss is due to a discrete nonhomogeneity within the primary range cell. For example, a large target within the test range cell but at a different angle and/or Doppler appears as a false alarm at the look angle-Doppler domain. Other examples include a strong discrete nonhomogeneity, such as a corner reflector, in the primary range cell. These false alarms appear through the sidelobes of the adapted beam pattern. The secondary data cells do not carry information about the discrete nonhomogeneity and hence a statistical algorithm cannot suppress discrete (uncorrelated) interference within the range cell under test.

IEEE Proceedings online no. 20000085

DOI: 10.1049/ip-rsn:20000085

Paper first received 24th March and in revised form 25th October 1999

The authors are with the Air Force Research Laboratory, Sensors Directorate, Signal Processing Branch, 26 Electronic Parkway, Rome, NY 13441-4514, USA

The inability of statistical STAP algorithms to counter nonhomogeneities in the primary data motivates research in the area of non-statistical or D^3 algorithms. These algorithms use data from the range cell of interest only, eliminating the sample support problems associated with statistical approaches. This approach has recently focused on one-dimensional spatial adaptivity [5–7]. This paper introduces a new two-dimensional space-time D^3 algorithm based on the one-dimensional algorithm of Sarkar *et al.* [7].

The main contribution of this paper is the introduction of a two-stage hybrid STAP algorithm combining the benefits of both non-statistical and statistical methods. The hybrid approach uses the non-statistical algorithm as a first-stage filter to suppress discrete interferers present in the range cell of interest. This first stage serves as an adaptive transform from the space-time domain to the angle-Doppler domain and so replaces the steering vector based non-adaptive transform used in Part 1 of this paper [8]. Modified joint domain Localised (JDL) statistical processing in the angle-Doppler domain is the second stage designed to filter out the residual correlated interference.

This research is a contribution to STAP and the broader field of knowledge-based STAP (KB-STAP). KB-STAP [9] chooses the best of many possible STAP algorithms for detection with knowledge-based control of algorithm parameters and selection of secondary data using NIDs. Currently KB-STAP architectures incorporate statistical algorithms only and a NHD is used to eliminate non-homogeneous range bins from the secondary data support. The problem of target detection within a nonhomogeneous range bin has not been addressed. This paper addresses this hitherto unsolved problem and therefore significantly enhances the practical relevance of KB-STAP, especially in dense target environments.

2 Two-dimensional direct data domain algorithm

Direct data domain algorithms use data from the range cell of interest only, eliminating the sample support problems associated with statistical approaches. This Section develops the new D^3 algorithm for the ideal case of a linear array of equispaced, isotropic, point sensors. Section 4.2 extends the formulation to account for mutual coupling and other non-ideal effects in real arrays.

Consider a N -element linear array, with interelement spacing d . The array is assumed to operate at a center frequency corresponding to wavelength λ . The array receives target, clutter and other interference returns corresponding to the M pulses per coherent pulse interval (CPI). These pulses are transmitted at a pulse repetition frequency f_R . The D^3 algorithm maximises the gain in the direction of the look azimuth angle ϕ_i and Doppler frequency f_i , while simultaneously minimising the residual interference power. This paper assumes the data has been pre-processed, including pulse compression.

To best present the D^3 algorithm, the data from N elements due to the M pulses in a CPI can be written as a $N \times M$ matrix X whose m th column corresponds to the N returns from the m th pulse, represented by $x(m)$. This matrix is a reshaping of the length NM -vector used in Part 1. The data matrix is a sum of the target and interference returns

$$X = \xi V + C + N \quad (1)$$

where ξ is the target amplitude, C is the matrix of external interference sources and N represents thermal noise. The space-time steering matrix V corresponds to the look angle ϕ_i and Doppler f_i , given in terms of the spatial steering vector a and the temporal steering vector b ([10], pp. 12–17).

The space-time steering matrix V is given by

$$z_s = e^{(j2\pi d/\lambda) \sin \phi_i} \quad (2)$$

$$z_t = e^{j2\pi f_i/f_R} \quad (3)$$

$$a(\phi_i) = [1 \quad z_s \quad z_s^2 \quad \dots \quad z_s^{(N-1)}]^T \quad (4)$$

$$b(f_i) = [1 \quad z_t \quad z_t^2 \quad \dots \quad z_t^{(M-1)}]^T \quad (5)$$

$$V = a(\phi_i) \otimes b^T(f_i) \quad (6)$$

$$= \begin{bmatrix} 1 & z_t & \dots & z_t^{(M-1)} \\ z_s & z_s z_t & \dots & z_s z_t^{(M-1)} \\ \vdots & \vdots & \ddots & \vdots \\ z_s^{(N-1)} & z_s^{(N-1)} z_t & \dots & z_s^{(N-1)} z_t^{(M-1)} \end{bmatrix} \quad (7)$$

where z_s represents the spatial phase progression from one element to the next and z_t represents the temporal phase progression from one pulse to the next. As in Part 1 $a(\phi_i)$ and $b(f_i)$ represent the spatial and temporal steering vectors, respectively. Again, the steering vector only sets the look direction ϕ_i and look Doppler f_i . In case a target is really present, there is a beam mismatch between target and steering vector.

Eqn. 7 indicates that, row by row, the signal component advances from one element to the next by a constant spatial multiplicative factor z_s for each pulse. Similarly, at each element the signal component advances from one pulse to the next by a constant temporal multiplicative factor z_t , indicated column to column. Therefore, the signal component is eliminated from terms such as $(X_{nm} - z_s^{-1} X_{(n+1)m})$ and $(X_{nm} - z_t^{-1} X_{n(m+1)})$, leaving only residual interference terms. D^3 methods use this fact to obtain adaptive weights that minimise the residual interference power [5, 7] within the primary range cell. Define the matrix B to be

$$B = \begin{bmatrix} X_{00} - z_t^{-1} X_{01} & X_{01} - z_t^{-1} X_{02} \\ X_{10} - z_t^{-1} X_{11} & X_{11} - z_t^{-1} X_{12} \\ \vdots & \vdots \\ X_{(N-1)0} - z_t^{-1} X_{(N-1)1} & X_{(N-1)1} - z_t^{-1} X_{(N-1)2} \\ \dots & X_{0(M-2)} - z_t^{-1} X_{0(M-1)} \\ \dots & X_{1(M-2)} - z_t^{-1} X_{1(M-1)} \\ \vdots & \vdots \\ \dots & X_{(N-1)(M-2)} - z_t^{-1} X_{(N-1)(M-1)} \end{bmatrix} \quad (8)$$

Theoretically the entries of the $N \times (M-1)$ matrix B carry interference terms only, but due to beam mismatch, there is some residual target information in the entries of B . However, unless the target is significantly off the look direction/Doppler, the target signal is effectively nulled. In the case where the target is significantly off the look direction, it must be treated as interference, in a surveillance radar, targets must be declared only if they are in the look direction. In fact, sidelobe targets are an example of the discrete interference that drives this research.

Consider the following scalar functions of a set of temporal weights w_t ,

$$G_{w_t} = |b_{(0:M-2)}^H w_t|^2 = w_t^H b_{(0:M-2)} b_{(0:M-2)}^H w_t \quad (9)$$

$$I_{w_t} = \|B^* w_t\|^2 = w_t^H B^T B^* w_t \quad (10)$$

$$R_{w_t} = G_{w_t} - I_{w_t} \quad (11)$$

where H represents the conjugate transpose, $*$ the complex conjugate, $\|\cdot\|_2$ the two-norm of a vector and $b_{(0:M-2)}$ the first $(M-1)$ entries of the temporal steering vector defined by eqn. 5. In eqn. 10, $B^* w_t$ is used to remain consistent with the term $b_{(0:M-2)}^H w_t$ in that the weights multiply the conjugate of the data.

The term G_{w_t} in eqn. 9 represents the gain of the weight vector w_t at the look Doppler frequency f_t while the term I_{w_t} in eqn. 10 represents the residual interference power after the data is filtered by the same weights. Hence, R_{w_t} in eqn. 11 represents the difference between the gain of the antenna at the look Doppler and the residual interference power. The new D^3 algorithm finds the weights that maximise this difference. Mathematically

$$\begin{aligned} \max_{\|w_t\|_2=1} R_{w_t} &= \max_{\|w_t\|_2=1} [G_{w_t} - I_{w_t}] \\ &= \max_{\|w_t\|_2=1} w_t^H [b_{(0:M-2)} b_{(0:M-2)}^H - B^T B^*] w_t \end{aligned} \quad (12)$$

where the constraint $\|w_t\|_2 = 1$ is chosen to obtain a finite solution. Using the method of Lagrange multipliers, it can be shown that the desired temporal weight vector is the eigenvector corresponding to the maximum eigenvalue of the $(M-1) \times (M-1)$ matrix $[b_{(0:M-2)} b_{(0:M-2)}^H - B^T B^*]$. This formulation yields a temporal weight vector of length $(M-1)$, representing the degree of freedom used to eliminate the target signal in eqn. (8).

Analogous to the temporal adaptive weights, the spatial weight vector w_s is the eigenvector corresponding to the largest eigenvalue of the $(N-1) \times (N-1)$ matrix $[a_{(0:N-2)} a_{(0:N-2)}^H - A^T A^*]$, where $a_{(0:N-2)}$ is the vector of the first $(N-1)$ entries of the spatial steering vector defined by eqn 4 and A is the $M \times (N-1)$ matrix

$$A = \begin{bmatrix} X_{00} - z_s^{-1} X_{10} & X_{10} - z_s^{-1} X_{20} \\ X_{01} - z_s^{-1} X_{11} & X_{11} - z_s^{-1} X_{21} \\ \vdots & \vdots \\ X_{0(M-1)} - z_s^{-1} X_{1(M-1)} & X_{1(M-1)} - z_s^{-1} X_{2(M-1)} \\ \dots & X_{(N-2)0} - z_s^{-1} X_{(N-1)0} \\ \dots & X_{(N-2)1} - z_s^{-1} X_{(N-1)1} \\ \vdots & \vdots \\ \dots & X_{(N-2)(M-1)} - z_s^{-1} X_{(N-1)(M-1)} \end{bmatrix} \quad (13)$$

Overall, the length MM space-time adaptive weight vector, for look angle ϕ_t and look Doppler f_t is then given by

$$w(\phi_t, f_t) = \begin{bmatrix} w_t \\ 0 \end{bmatrix} \otimes \begin{bmatrix} w_s \\ 0 \end{bmatrix} \quad (14)$$

The zeros appended to the spatial and temporal weight vectors represent the lost degree of freedom in space and time. This D^3 algorithm differs from other non-statistical algorithms by maximising the mainbeam gain in the look direction as opposed to maintaining the gain at some chosen level.

2.1 Trade-off between mainbeam gain and interference suppression

In Section 2, the temporal adaptive weights are chosen from the eigenvectors of the matrix B so as to maximise the difference between the mainbeam gain of the antenna G_{w_t} and the residual interference power I_{w_t} . It is possible to emphasise one or the other term by introducing a new parameter κ . Consider the scalar expression

$$\begin{aligned} \max_{\|w_t\|_2=1} R_{w_t}(\kappa) &= \max_{\|w_t\|_2=1} [G_{w_t} - \kappa^2 I_{w_t}] \\ &= \max_{\|w_t\|_2=1} w_t^H [b_{(0:M-2)} b_{(0:M-2)}^H - \kappa^2 B^T B^*] w_t \end{aligned} \quad (15)$$

Choosing $\kappa=0$ eliminates the interference term leaving the largest eigenvalue equal to $\|b_{(0:M-2)}\|_2^2 = (M-1)$ with the corresponding eigenvector $w_t = b_{(0:M-2)} / \|b_{(0:M-2)}\|_2$. Therefore, as $\kappa \rightarrow 0$ the D^3 weight vector approaches the non-adaptive steering vector used in Part 1 of this paper.

On the other hand if κ is chosen to be large, the role of the term G_{w_t} is negligible and the weight vector is dependent on the interference terms only. This leads to emphasis on the suppression of interference at the expense of mainbeam gain. In this case, the look direction plays a limited role through the term z_t in eqn. 8 and the weight vector may vary significantly by range cell.

3 Two-stage hybrid algorithm

The main thrust of this paper is the presentation of a new hybrid approach to STAP combining the benefits of both D^3 and statistical methods. The application of interest is the suppression of discrete nonhomogeneities within the range cell under test. This problem is particularly significant because statistical methods cannot suppress such nonhomogeneities, which then appear as false alarms through the sidelobes of the adapted beam pattern. For example, a large target within the test range cell, but at a different angle and/or Doppler, may be incorrectly detected at the look angle/Doppler. Other examples include a corner reflector within the range cell of interest.

Consider the general framework of any STAP algorithm. The algorithm processes received data to obtain a complex weight vector for each range bin and each look angle/Doppler. The weight vector then multiplies the primary data vector to yield a complex number. The process of obtaining a real scalar from this number for threshold comparison is part of the post-processing and not inherent in the algorithm itself. The adaptive process therefore estimates the signal component in the look direction and hence the adaptive weights can be viewed in a role similar to the non-adaptive steering vectors, used in Part 1 of this paper to transform the space-time data to the angle-Doppler domain.

The D^3 processing algorithm begins with a transformation of the data from the space-time domain to the angle-Doppler domain. This is followed by statistical adaptive processing within a localised processing region (LPR) in the angle-Doppler domain. Part 1 of this paper represents the transformation process as a multiplication with a general transformation matrix T . The hybrid approach uses the D^3 weights, replacing the non-adaptive steering vectors used earlier. By choosing the set of look angles and Dopplers to be points in the LPR, the D^3 weights perform a function analogous to the non-adaptive transform.

The D^3 algorithm serves as an *adaptive* transformation from the space-time domain to the angle-Doppler domain.

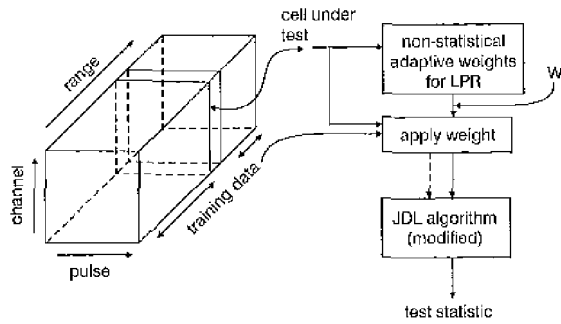


Fig. 1 Two-stage hybrid algorithm block diagram

JDL statistical processing in the angle–Doppler domain forms the second stage of adaptive processing to filter the residual correlated interference. The block diagram of the proposed two-stage hybrid algorithm is shown in Fig. 1. The D^3 algorithm is used repeatedly with the η_a look angles and η_d look Doppler frequencies to form the LPR. The space–time data is transformed to the LPR in the angle–Doppler domain using these adaptive weights. Using the D^3 weights from eqn. 14, the transformation matrix presented in Part I for the LPR covering three angle bins ($\phi_{-1}, \phi_0, \phi_1$; $\eta_a=3$) and three Doppler bins (f_{-1}, f_0, f_1 ; $\eta_d=3$) is now given by

$$T = [\begin{matrix} w(\phi_{-1}, f_{-1}) & w(\phi_0, f_{-1}) & w(\phi_1, f_{-1}) \\ w(\phi_{-1}, f_0) & w(\phi_0, f_0) & w(\phi_1, f_0) \\ w(\phi_{-1}, f_1) & w(\phi_0, f_1) & w(\phi_1, f_1) \end{matrix}] \quad (16)$$

The crucial difference between the hybrid algorithm and the JDL algorithm detailed in Part I of this paper is that such an adaptive transformation is noninvertible, resulting in some information loss. However, this information loss may be beneficial. The hybrid algorithm takes advantage of this loss to suppress discrete interferers within the range cell of interest. The framework presented in Part I of the paper also accounts for the spread in target information into all angle–Doppler bins in the LPR. The advantages associated with the JDL algorithm, such as in reduction in the required secondary data support, carry over to the hybrid algorithm.

The same transformation matrix T is used to transform the primary and secondary data to the angle–Doppler domain. Unlike the JDL algorithm this transformation matrix changes from range cell to range cell. The hybrid algorithm forms the adaptive transformation matrix as given by eqn. 16 for each range cell and then transforms this primary and associated secondary data to the angle–Doppler domain. This process is repeated for each range cell.

4 Numerical examples

This Section presents three examples to test the hybrid algorithm presented in Section 3. As in Part I, the examples include simulated data from an ideal array of isotropic point sensors and also measured data from the MCARM program.

4.1 Simulated data

The hybrid algorithm may be applied to homogeneous data, though this is not the application of interest. The algorithm is specifically designed to suppress the effects of discrete nonhomogeneities within the primary range cell.

Therefore the approach taken here is not to present the probability of detection for a chosen probability of false alarm. A more fruitful test is to compare the adapted beam patterns associated with the three algorithms discussed in this paper: the JDL algorithm of Part I, the new D^3 algorithm and the hybrid algorithm. The beam patterns illustrate the performance of the hybrid algorithm in suppressing discrete nonhomogeneities and correlated interference.

In Part I, the angle–Doppler weights are obtained using $\tilde{w} = \tilde{R}^{-1} \tilde{v}$, based on an estimated angle–Doppler covariance matrix \tilde{R} and angle–Doppler steering vector \tilde{v} . The equivalent space–time adaptive weights are given by

$$w = T \tilde{w} \quad (17)$$

These equivalent space–time weights may be used to obtain adapted beam pattern plots.

As in Part I, the simulated data is generated using the physical model developed by Jaffer *et al.* [11] and Ward [10]. The model generates homogeneous data and a discrete nonhomogeneity is later added to the homogeneous data as a strong return from an angle and/or Doppler different from the look angle/Doppler.

The simulation includes the effects of clutter, white noise, two barrage noise jammers and a discrete interferer. Table 1 lists the parameters used in the example. The jammer and interferer powers are referenced to the noise level. The clutter power is fixed by the transmit power and the assumed land reflectivity. The jammers and the clutter represent correlated interference because these two sources of interference are homogeneous across all range cells. Note that the discrete interferer is within the target range

Table 1: Parameters for example using simulated data

Parameter	Value
Elements (M)	18
Element spacing	0.5 λ
Array transmit pattern	uniform
Mainbeam transmit azimuth	0 deg
Land reflectivity	-3.0 dB
Transmit power	400 kW
Backlobe attenuation	30
Jammer azimuth angles	$[-20^\circ, 45^\circ]$
Target normalised Doppler (f_t)	1/3
Doppler of interferer	1/3
Interferer power	40 dB
Number of Doppler bins in LPR	3
$(d/\lambda) \sin \phi$	$1/\sqrt{M}$
Pulses (M)	18
Pulse repetition frequency	300 Hz
Uncompressed pulse width	400 μ s
β (Clutter slope)	1
Number of clutter patches	361
Jammer powers	[40 dB 40 dB]
Thermal noise power	unity
Jammer elevation angles	$[0^\circ, 0^\circ]$
Target azimuth (ϕ_t)	0°
Angle of interferer	-51°
Emphasis parameter κ	$\sqrt{1/M}$
Number of angle bins in LPR	3
Δf	$1/M/2$

cell only, with an offset in angle but not Doppler. Matching the nonhomogeneity to the target in one domain makes it more difficult for the algorithm to suppress the nonhomogeneity. The Table also lists the parameters used by the hybrid algorithm including the emphasis parameter κ . The final line in the Table refers to the spacing between the angle and Doppler bins in the LPR which comprises three angles and three Doppler frequencies centred around the look direction. The number of secondary data vectors used to estimate the covariance matrix in the second stage JDL processing is set to $2(\text{DOF})=18$.

The adapted beam pattern plots presented in this paper are the mean patterns over 200 independent realisations. Vertical bars represent the standard deviation over these 200 trials. This method was required because the D^3 algorithm is non-statistical and based solely on a single data set/realisation. Operating with the known covariance matrix to obtain an ideal pattern, as possible in statistical algorithms, is not an option.

Figs. 2 and 3 illustrate the antenna patterns along the target azimuth and Doppler for the JDL algorithm described in Part 1 of this paper. Note the high sidelobe in the direction of the discrete interferer. The discrete interferer is within the primary range cell and so does not contribute to the covariance matrix estimate and is therefore not nulled by a purely statistical algorithm such as JDL. However, as Fig. 2 shows, the JDL algorithm does place deep nulls in the direction of the jammers at -20° and 45° . Fig. 3 shows the deep null placed at zero Doppler

frequency corresponding to mainbeam clutter. These two Figures illustrate the effectiveness of the JDL algorithm in suppressing correlated interference such as barrage noise jamming and clutter.

Figs. 4 and 5 plot the antenna patterns resulting from the implementation of the two-dimensional D^3 algorithm. Fig. 4 shows that the D^3 algorithm places a null in the direction of the discrete interferer. The algorithm is effective in countering a discrete interferer within the range cell of interest. The adapted spatial beam pattern shows a distinct null in the direction of the discrete interferer at -51° . However, Figs. 4 and 5 also illustrate the limitations of the D^3 algorithm. The nulls in the direction of the jammers are not as deep as in the case of JDL in Fig. 2. Fig. 5 shows the null at $\omega=0$ in the Doppler spectrum and is also not as deep as in Fig. 5, i.e. the mainbeam clutter is not suppressed as effectively as by the JDL algorithm.

Figs. 6 and 7 plot the antenna beam patterns resulting from the use of the hybrid algorithm. Fig. 6 shows that the hybrid algorithm combines the advantages of both statistical and non-statistical adaptive processing. The adapted azimuth pattern shows deep nulls at -51° , -20° and 45° , the directions of the discrete interferer and the two jammers. Fig. 7 shows that the adapted pattern has a deep null at $\omega=0$ resulting in effective nulling of the mainbeam clutter. The hybrid algorithm therefore suppresses correlated interference such as clutter and jamming and also uncorrelated interference such as the strong interferer in the primary range cell.

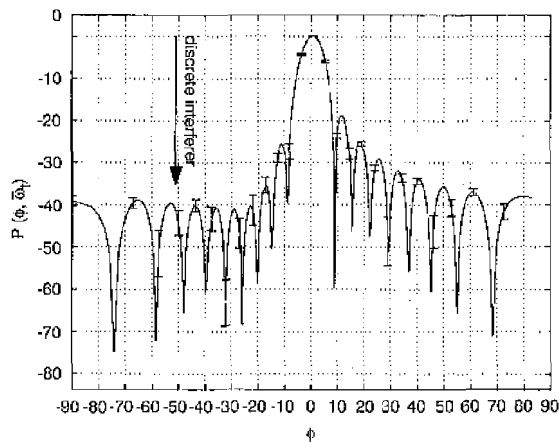


Fig. 2 JDL algorithm antenna pattern at the target Doppler

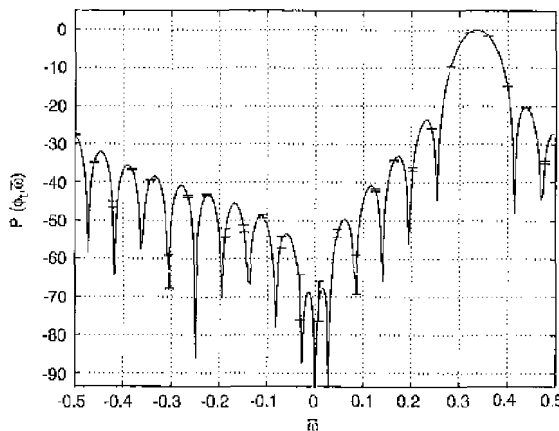


Fig. 3 JDL algorithm antenna pattern at the target azimuth

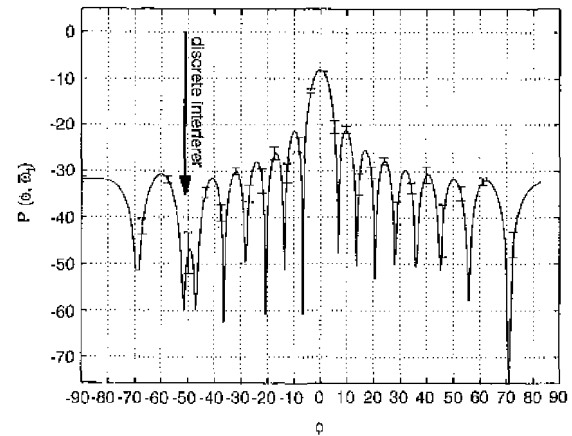


Fig. 4 Direct data domain algorithm antenna pattern at the target Doppler

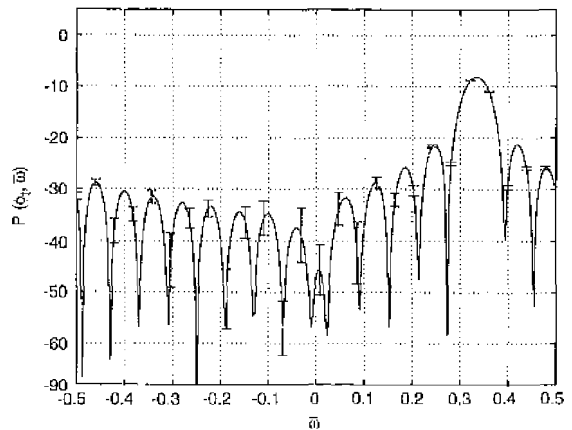


Fig. 5 Direct data domain algorithm antenna pattern at the target azimuth

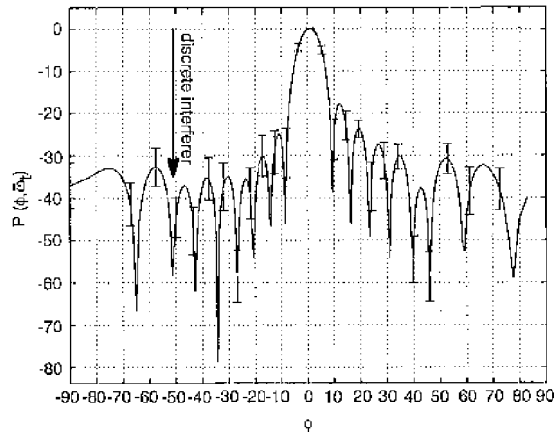


Fig. 6 Hybrid algorithm antenna pattern at the target Doppler

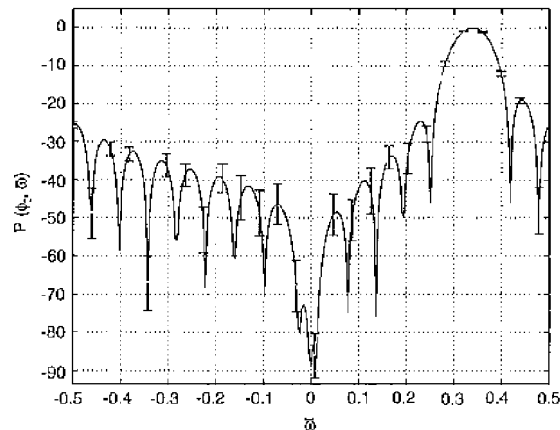


Fig. 7 Hybrid algorithm antenna pattern at the target azimuth

4.2 Measured data

This Section presents two examples of the application of the hybrid algorithm to measured data. The examples use data from the multi channel airborne radar measurements (MCARM) [12] database as described in Part 1. The examples use the same two acquisitions (acquisitions 575 and 152 on flight 5) to illustrate the suppression of discrete interference in measured data. Descriptions of these two acquisitions are available in Part 1.

4.2.1 Application of the hybrid method to measured data: The D^3 method was developed in Section 2 for an equispaced, linear array of point sensors. This allowed for the assumption of no mutual coupling between the elements and the simplified spatial steering vector given by eqn. 4. This in turn allowed the crucial assumption that for each pulse the signal component advances from one element to the next by a constant spatial multiplicative factor z_s .

The MCARM antenna is an array of 22 elements arranged in a rectangular 2×11 grid [12]. For a rectangular array, eqn. 4 is invalid. Furthermore, the elements of all real arrays sample and re-radiate the incident fields, leading to mutual coupling between the elements. In this case, the spatial steering vector must be measured or evaluated using a numerical electromagnetic analysis. Provided with the MCARM database is a set of measured spatial steering vectors for some chosen azimuth and elevation angles.

Ignoring mutual coupling degrades the performance of any STAP algorithm [13–15]. As illustrated in Part 1 through the implementation of measured steering vectors, accounting for mutual coupling significantly enhances statistical algorithm performance. D^3 algorithms are based entirely on the assumption of a linear array of point sensors, allowing mutual coupling to severely affect performance [13, 14]. The authors in [14] use a method of moments (MOM) numerical electromagnetic analysis of the array to evaluate the mutual coupling matrix and compensate for these effects. Unfortunately a MOM analysis of the MCARM antenna is not available and the compensation procedure of [14] cannot be used.

Instead of a compensation method based on numerical electromagnetic analysis, this paper applies the D^3 algorithm to the MCARM data using an *ad hoc* procedure. Eqs. 2 and 4 indicate that the spatial steering vector at broadside ($\phi = 0$) is given by $\mathbf{a}(\phi = 0) = [1 \ 1 \cdots 1 \ 1]^T$. In the absence of mutual coupling, this steering vector at broadside is valid for arrays in any configuration. The approach then is to artificially rotate all the data, using the measured spatial steering vector, so as to force the look direction to broadside. This compensates for the rectangular array configuration and also the mutual coupling associated with the look direction. The rotation is achieved by an entry-by-entry division of the received voltages at the array level with the measured spatial steering vector corresponding to the look direction. Using pseudo-MATLAB[®] notation, this operation can be represented by

$$\bar{\mathbf{x}}(m) = \mathbf{x}(m) ./ \mathbf{a}_m(\phi_l) \quad (18)$$

where $\mathbf{x}(m)$ represents the N returns from the m th pulse in a CPI and $\mathbf{a}_m(\phi_l)$ represents the measured steering vector corresponding to the look direction ϕ_l . This operation is repeated for all pulses in all range bins.

The division operation of eqn. 18 forces the effective spatial steering vector for any look direction to be $\mathbf{a}(\phi_l) = [1 \ 1 \cdots 1 \ 1]^T$, equivalent to broadside in an ideal array. The hybrid method as developed in Section 3 is therefore applied to the ‘rotated’ data $\bar{\mathbf{x}}$ with broadside as the look direction.

4.2.2 Example 1. Injected target: The first example uses the same scenario as in example 1 of Part 1. In this example, a discrete nonhomogeneity is introduced into the data by adding a strong fictitious target at a single range bin, but not at the look angle–Doppler. Two cases are considered within this example; no injected target and an injected weak target. The first case illustrates the suppression of the discrete nonhomogeneity. In the second case, a weak target is injected at the same range bin as the nonhomogeneity, but at a different angle and Doppler. This case illustrates the ability of the hybrid algorithm to detect weak targets in the presence of strong discrete nonhomogeneities. In this case, only 22 of the 128 pulses in the CPI are used, i.e. $N = 22$, $M = 22$. The value of the emphasis parameter is chosen to be $\kappa = (NM)^{3/2}$.

The details of the nonhomogeneity and the weak target are shown in Table 2.

The hybrid algorithm is applied to the data from the range bin with the nonhomogeneity and surrounding range bins. The output MSMI statistic from the second stage of the hybrid algorithm is plotted as a function of range. In this example, five Doppler bins and five angle bins form the LPR for both the JDL algorithm and the second stage of the hybrid algorithm. The number of secondary data

Table 2: Parameters for example using MCARM data

Parameter	Nonhomogeneity	Target
Amplitude	0.0241	0.000241
Angle bin	35	65 (broadside)
Doppler bin	-3	-2
Range bin	290	290

vectors used to form an estimate of the covariance matrix is set at $4(\text{DOF}) = 100$.

For the case without an injected target, Fig. 8 compares the output from the JDL algorithm developed in Part. 1 with the output of the hybrid algorithm. As can be seen, the JDL algorithm indicates the presence of a large target in the look direction. This is because the large nonhomogeneity at angle bin 35 and Doppler bin -3 is not suppressed by the statistical algorithm, leading to false alarms at the look direction. On the other hand, the hybrid algorithm shows no target at broadside. The nonhomogeneity is suppressed in the first D^3 stage and residual clutter is suppressed in the second JDL stage.

A fictitious target injected at the look direction and Doppler illustrates the sensitivity of the hybrid algorithm to weak targets. The parameters of the weak target are listed in Table 2. Fig. 9 compares the output of the two algorithms in the case of an injected weak target. The JDL algorithm again shows the presence of a strong target in the look direction. However from Fig. 8, the strength of the statistic is caused by the nonhomogeneity. The output of the hybrid method shows the statistic at the target range bin is 6.9 dB above the next highest false alarm algorithm.

This example shows that the hybrid algorithm may be used to detect a weak target in the presence of a discrete nonhomogeneity within the range cell of interest.

4.2.3 Example 2. MTS tones: As explained in Part 1, certain acquisitions within the MCARM database include signals from a moving target simulator (MTS) at known Doppler shifts. A brief description of the MTS is available in Part 1. In acquisition 152 on flight 5, the MTS tones occur in angle bin 59. In this example, the look direction is set to angle bin 85 for a mismatch and the JDL and hybrid algorithms are applied to the same acquisition. For this look direction, the MTS tones at angle bin 59 act

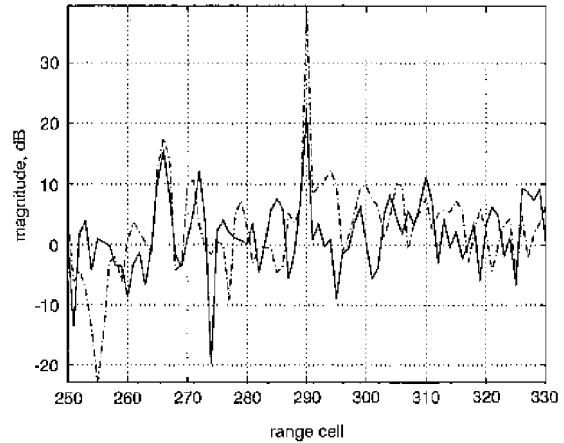


Fig. 9 Data with nonhomogeneity and injected target

— hybrid
 - - - JDL

like strong targets at a different angle bin, i.e. discrete nonhomogeneities. As in Example 1, two cases are considered; no injected target and a weak injected target. The first case illustrates the suppression of the MTS tones acting as discrete, strong nonhomogeneities. The second case illustrates the sensitivity of the hybrid algorithm to weak targets. This example uses all 128 pulses in the CPI, i.e. $N=22$, $M=128$. The emphasis parameter for the direct data domain method is set to a large value of $\kappa = (NM)^{3/2}$.

In acquisition 152 of flight 5, the MTS tones are in range bin 449-450 with the strongest tone at a Doppler corresponding to bin -53 and angle bin 59. The example focuses on the suppression of this tone. Fig. 10 plots the MSM1 statistic of the two algorithms for the case without an injected target. Only measured data is used, without any artificial injected targets. The JDL algorithm detects a large target at range bins 449 and 450. This false alarm is due to the strong MTS tone at angle bin 59 even though the look direction is set at angle bin 85. The hybrid algorithm, however, suppresses the strong MTS tone, showing no activity at range bins 449 and 450.

Fig. 11 plots the results of using the two algorithms to detect a weak target injected into range bin 450. The parameters of the weak target are; magnitude: 0.0001, Doppler bin: -53, angle bin: 85. This weak target is

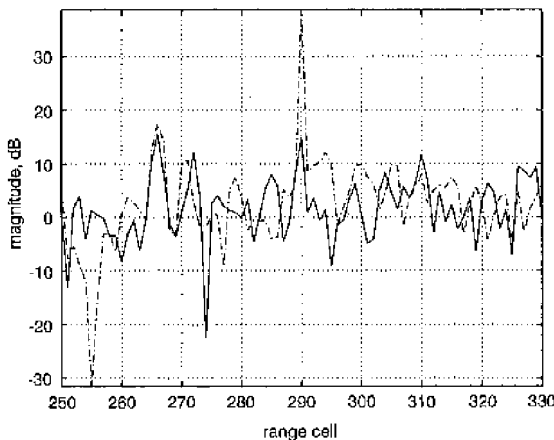


Fig. 8 Data with nonhomogeneity, but without injected target

— hybrid
 - - - JDL

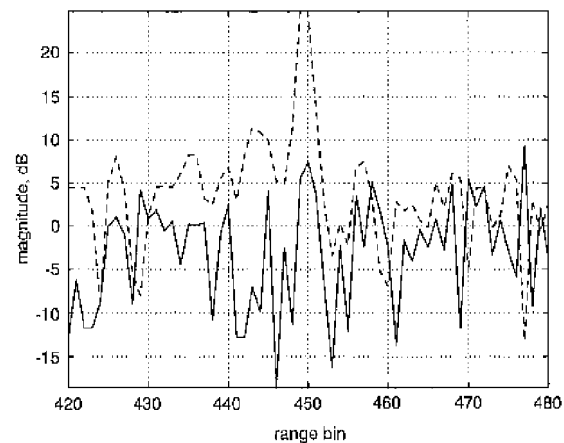


Fig. 10 Data with MTS tones, without injected target

— hybrid
 - - - JDL

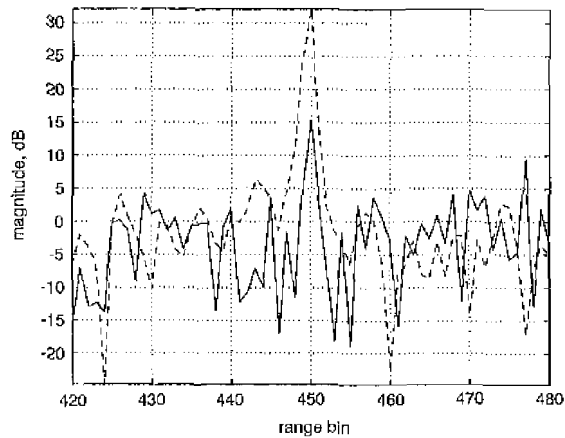


Fig. 11 Data with MTS tones and injected target

— hybrid
 --- JDL

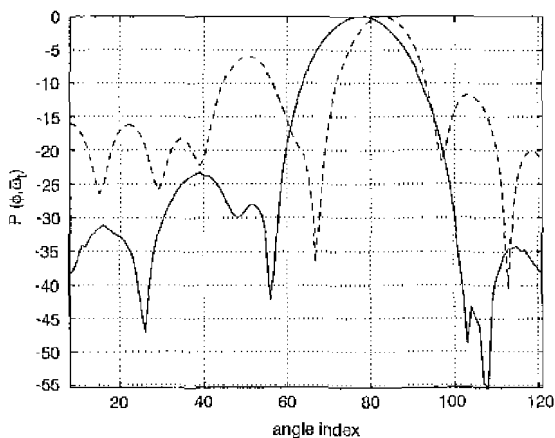


Fig. 12 Beam patterns of the JDL and hybrid algorithm using MCARM data with MTS tones

— hybrid
 --- JDL

easily detected by the hybrid algorithm with the statistic at the target range bin 9.8 dB above the nearest false alarm.

The beam patterns associated with the two algorithms illustrate the improvement in using the D^3 algorithm as the first stage of a two-stage hybrid method. Fig. 12 plots the spatially adapted beam pattern at the look Doppler frequency for the JDL and hybrid algorithms. The plot for the hybrid algorithm shows the deep null in the adapted pattern of the hybrid algorithm near angle bin 57 while the JDL pattern does not show such a null. In applying the JDL algorithm to the MCARM data acquisition with MTS tones, the strong tones leak through the sidelobes of the adapted pattern, leading to false alarms.

5 Knowledge-based STAP

This two-part paper details how the two-stage algorithm is crucial for practical space-time adaptive processing for airborne radar applications, accounting for both homogeneous and nonhomogeneous interference scenarios. Traditional statistical STAP schemes are effective when the data cube is homogeneous, i.e. the statistics of the secondary data accurately reflect the statistics of the interference

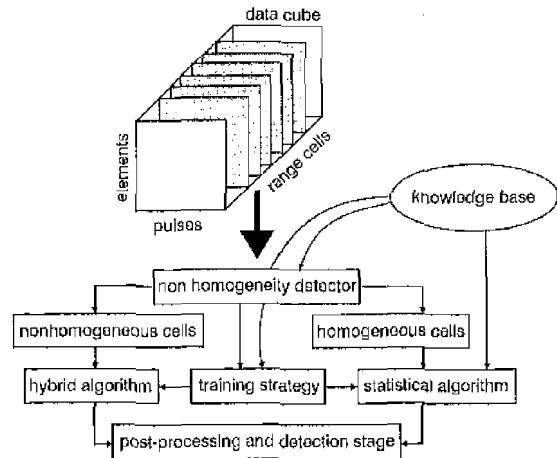


Fig. 13 Multi-pass knowledge-based STAP processing for airborne radar

within the primary range cell. The performance of these statistical schemes suffers significantly when the secondary data is nonhomogeneous with respect to the primary data.

The envisioned knowledge-based STAP processing is illustrated in Fig. 13. The first pass through the data cube identifies range cells that are nonhomogeneous with respect to the data cube. This NIID identifies the statistical 'outliers'. The figure of merit may be the generalised inner product or the output statistic from a STAP algorithm such as the MSMI-NHD [1–4]. In either case, statistical outliers are declared to be nonhomogeneous. A knowledge base may be used to define the term 'outlier' [9]. This knowledge base may possess information regarding the terrain, interfering discretets, manmade interference sources, etc. For example, when flying over a homogeneous area such as a desert, the knowledge base can set a stringent definition for an 'outlier'. However, urban areas may result in many range cells being declared nonhomogeneous. The knowledge base can be updated in real time.

Once the range cells are separated into homogeneous and nonhomogeneous categories, the second pass through the data cube applies the statistical algorithm for the homogeneous range cells and the two-stage hybrid algorithm for nonhomogeneous range cells. Within the homogeneous range cells, the knowledge base informs the decision of which statistical STAP algorithm to employ. The factors involved in the decision include required speed of computation, availability of secondary data, etc. For example, over benign terrain it may be possible to use the extended factored time-space (EFTS) requiring a large number of secondary data samples. However, in more challenging scenarios the JDL algorithm of Part 1 may be used. This algorithm requires relatively few secondary data samples. The knowledge base also impacts the decision as to the choice of the secondary data used in estimating the covariance matrix.

In the case of the range cells declared nonhomogeneous, the choice is limited. The two-stage hybrid algorithm detailed in this paper is probably the only published effort regarding detection of targets in nonhomogeneous range cells. The second stage of this algorithm uses transform domain localised processing allowing the knowledge base to determine the secondary data used in estimating the transform domain covariance matrix.

In summary, a practical approach to STAP might use multi-pass processing to account for nonideal, nonhomo-

geneous interference scenarios. Depending on the scenario at hand, and with the help of a knowledge base, the appropriate STAP algorithm will maximise the probability of detecting and identifying weak targets.

KB-STAP is, as yet, an open research topic and necessarily an amorphous concept. In its final implementation KB-STAP will include several STAP algorithms, scene information, information from other sensors and heuristics to choose between the available approaches. However, current implementations of the KB-STAP concept are simplistic and limited. Research is underway to consolidate the related concepts and process the immense amount of information in real time.

6 Conclusions

This paper develops two new algorithms; a two-dimensional, non-statistical approach to STAP and a hybridisation of this approach with statistically based methods. The non-statistical algorithm represents a significant advance on previously published work in this research area. This algorithm allows for the filtering of discrete interference within the range cell of interest. This feature enhances the true detection of weak targets in nonhomogeneous interference scenarios, while minimising false alarms. Statistical algorithms cannot suppress discrete nonhomogeneities because the secondary data possesses no information regarding such interference. However, performance of direct data domain algorithms in homogeneous interference scenarios is inferior to traditional statistical STAP algorithms. Each of these two approaches to STAP has its own area of application.

The proposed two-stage hybrid algorithm alleviates this drawback by implementing a second stage of statistical processing after using the D^3 algorithm as an adaptive transform to the angle-Doppler domain. This algorithm combines the advantages of both the statistical and non-statistical approaches. The D^3 method is particularly effective at countering nonhomogeneous interference. The statistical STAP algorithm then improves on the suppression of the residual correlated interference.

The examples presented in Section 4 highlight the features of the new hybrid algorithm. The Section presents examples using simulated data and also measured data from the MCARM database. In the case of simulated data, the adapted beam patterns illustrate the ability to place deep pattern nulls in the direction of both correlated interference such as jammers and also discrete interference such as a large target in the range cell of interest.

Even with *ad hoc* compensation for mutual coupling, the hybrid algorithm shows a significant improvement over statistical methods in suppressing discrete nonhomogeneities. We anticipate a true evaluation of the mutual coupling would improve the performance of the hybrid algorithm.

In summary, this two-part paper presents a comprehensive approach to STAP and the broader field of knowledge-based STAP. Part 1 focuses on the well known joint domain localised processing algorithm. Reformulating the JDL algorithm significantly improves performance in both the ideal and real worlds. The use of a transformation matrix

removes restrictions placed on the algorithm by the original formulation.

Part 2 presents a new direct data domain algorithm and a hybridisation of the algorithm with JDL. This new hybrid algorithm gives the capability to perform STAP within nonhomogeneous range cells. This algorithm draws on the new formulation of JDL presented in Part 1.

The multi-pass approach significantly enhances the practicality of knowledge-based STAP for airborne surveillance applications. The envisioned system requires multi-pass processing to obtain some important information about the interference scenario. The first pass is a non-homogeneity detector followed in the second pass by appropriate STAP processing. The STAP stage can either draw from traditional algorithms in homogeneous environments or on the hybrid algorithm in nonhomogeneous environments. The decision to use one or the other approach will be informed by any available *a priori* information about the interference scenario.

7 References

- 1 CHANG, H.H.: 'Improving space-time adaptive processing (STAP) radar performance in nonhomogeneous clutter'. PhD thesis, Syracuse University, August 1997
- 2 MELVIN, W.L., and WICKS, M.C.: 'Improving practical space-time adaptive radar'. Proceedings of the 1997 IEEE National Radar Conference, May 1997, Syracuse, NY, USA
- 3 WICKS, M.C., MELVIN, W.L., and CHEN, P.: 'An efficient architecture for nonhomogeneity detection in space-time adaptive processing airborne early warning radar'. Proceedings of the 1997 International Radar Conference, October 1997, Edinburgh, UK, pp. 295-299
- 4 ADVE, R.S., HALE, T.B., and WICKS, M.C.: 'Transform domain localized processing using measured steering vectors and non-homogeneity detection'. Proceedings of the 1999 IEEE National Radar Conference, Apr. 1999, Boston, MA, USA, pp. 285-290
- 5 SARKAR, T.K., and SANGRUJI, N.: 'An adaptive nulling system for a narrow-band signal with a look-direction constraint utilizing the conjugate gradient method', *IEEE Trans. Antennas Propag.*, 1989, 37, pp. 940-944
- 6 PARK, S., and SARKAR, T.K.: 'A deterministic eigenvalue approach to space time adaptive processing'. Proceedings of the IEEE Antennas and Propagation Society International Symposium, July 1996, pp. 1168-1171
- 7 SARKAR, T.K., NAGARAJA, S., and WICKS, M.C.: 'A deterministic direct data domain approach to signal estimation utilizing non-uniform and uniform 2-d arrays', *Digit. Signal Process.*, 1998, 8, pp. 114-125
- 8 ADVE, R.S., HALE, T.B., and WICKS, M.C.: 'Practical joint domain localised adaptive processing in homogeneous and nonhomogeneous environments. Part I: Homogeneous environments', *IEE Proc., Radar Sonar Navig.*, 2000, 147, (2), pp. 57-65
- 9 ANTONIK, P., SCHUMAN, H.K., MELVIN, W.L., and WICKS, M.C.: 'Implementation of knowledge based control for space-time adaptive processing'. Proceedings of the 1997 International Radar Conference, October 1997, Edinburgh, UK, pp. 478-482
- 10 WARD, J.: 'Space-time adaptive processing for airborne radar'. MIT Lincoln Laboratory, Tech. Rep. F19628-95-C-0002 December 1994
- 11 JAFFER, A., BAKER, M., BALLANCE, W., and STAUB, J.: 'Adaptive space-time processing techniques for airborne radars'. Contract F30602-89-D-0028, Hughes Aircraft Company, Fullerton, CA 92634, USA, July 1991
- 12 SLOPER, D., FLENNER, D., ARNTZ, J., and FOGLE, E.: 'Multi-channel airborne radar measurement (MCARM), MCARM flight test'. Contract F30602-92-C-0161, Westinghouse Electronic Systems April 1995, Additional information available at <http://sunrise.deepthought.h.af.mil>
- 13 ADVE, R.: 'Elimination of the effects of mutual coupling in adaptive thin wire antennas.' PhD thesis, Syracuse University, December 1996
- 14 ADVE, R.S., and SARKAR, T.K.: 'Compensation for the effects of mutual coupling on direct data domain algorithms', *IEEE Trans. Antennas Propag.*, scheduled for publication December 1999
- 15 GUPTA, I., and KSIENSKI, A.: 'Effect of mutual coupling on the performance of adaptive arrays', *IEEE Trans. Antennas Propag.*, 1983, 31, pp. 785-791